CONCRETE LIBRARY OF JSCE NO. 20, DECEMBER 1992

DEVELOPMENT OF RC DISCRETE CRACK MODEL UNDER REVERSED CYCLIC LOADS AND VERIFICATION OF ITS APPLICABLE RANGE

(Rewritten in English of papers in Proceedings of the Japan Society of Civil Engineers, No.442/V-16, Feb. 1992.)

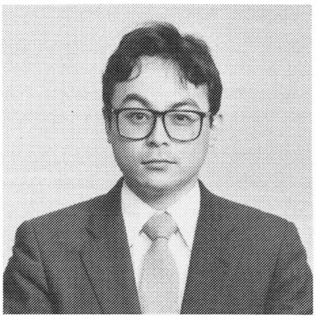

Tetsuya MISHIMA

Koichi MAEKAWA

SYNOPSIS

This paper aims to develop a RC discrete crack model under reversed cyclic loading, which is composed of a reinforcement part and a concrete part. The concrete model is proposed to be based on the generalized contact density model which has been examined under various sorts of loading paths and the criterion of crack occurrence. The reinforcement part is based on the steel strain-slip model. The cyclic steel strain-slip model after yielding is formulated by considering both inelastic and plastic zones in addition to dealing with the effect of adjacent cracks. The versatility of the discrete crack model to the structural crack planes is mainly checked through the comparison of RC plates. The accuracy for estimating the shear capacity of a RC crack is also verified by pure shear tests such as push-off tests.

Keywords: RC discrete crack model, reversed cyclic loading, RC plates, shear transfer , steel slip, shear capacity

T. Mishima is a research engineer at Technical Research Institute, Maeda Corporation, Tokyo, Japan. He received his Doctor of Engineering degree from the University of Tokyo in 1992. His research interests include nonlinear FEM analysis of reinforced concrete members, shear transfer mechanism along crack surfaces and construction joints, and thermal stress analysis of mass-concrete structures.

K. Maekawa is an associate professor in the Department of Civil Engineering at the University of Tokyo, Tokyo, Japan. He received his Doctor of Engineering degree in 1985 from the University of Tokyo. His research interests include constitutive models for concrete, cracks and reinforced concrete in-plane elements, structural analysis of reinforced concrete and development of high-performance concrete.

1 INTRODUCTION

Finite-element models of reinforced concrete structures can largely be divided into smeared crack models, which are formulated based on the average behavior of members, and discrete crack models, which are formulated based on individual cracks[1]. Finite elements based on a smeared crack model are suitable for members in which many cracks occur and the stress gradient is relatively gentle, such as the wall portions of shear walls. A discrete crack model is suitable for members whose behavior is governed by a small number of cracks or for the purpose of expressing the behavior of joints of members. Shin et al.[2] and Shin[3] successfully analyzed the restoring force characteristics and the ductility of shear walls accurately by applying a smeared crack model to walls and applying joint elements to joints in shear walls. These joint elements can be obtained by modeling the slippage[4] of reinforcing steel out of a crack surface and the mechanism of stress transfer[5] due to the interaction of aggregate along the crack surfaces. A major characteristic of these joint elements is that they can be applied to cyclic loading[3].

The model proposed by Shin et al. has already been verified by the measurement of the local behavior of joints in shear walls[2], and the model is highly reliable. The model, however, is not designed for application to cases where reinforcing steel and cracks cross at some angles. In addition, the deformation history expressed by the model was verified on the assumption that either the crack width or the shear slip varies substantially and variations of the other displacement components are relatively small. If the applicability of the model is to be expanded, it is desirable that it be expanded so that it can be applied to cracks in the ordinary portions of reinforced concrete members.

The goal of this study is to generalize material models constituting the proposed discrete crack model on the basis of the results of a uniaxially reversed cyclic loading test [6] on reinforced concrete plates, which was newly carried out in this study, designed to investigate behavior at the joint element level. When a discrete crack model is applied to cracks governing the global behavior of members, the crack surface and reinforcing steel often cross at some angle and the deformation process of the crack surface often include a complicated mixture of shear slip and opening. Slip characteristics of reinforcing steel might be affected by adjacent cracks. These factors have been considered in constructing material models.

As a result, the steel strain-slip model[3] proposed by Shin was expanded so that it could be applied to diagonal reinforcement. At the same time, a model applicable to reversed cyclic loading after yielding of reinforcing steel, in which the ranges of slip back during and after plastic deformation due to compression, was developed. With respect to a concrete model, the concept of Li-Maekawa's contact density function[5] was used to construct a generalized contact density model[7] with enhanced accuracy in shear-slip-opening modes under small restraint. Thus, the applicability of the discrete crack model including cracking conditions was expanded.

2 MATERIAL MODELS CONSTITUTING THE RC DISCRETE CRACK MODEL

2.1 Basic model of discrete crack

Figure 1 illustrates a discrete crack considered in this study. The crack considered here is a model of a crack in a reinforced concrete member and a joint of reinforced concrete members. The angle between reinforcement and the crack is represented by θ. Uniform distribution of reinforcement in the discrete crack section is assumed so that the reinforcement can be considered as a virtual continuum, as with a smeared crack model.

With respect to the mechanism of resistance of a crack in reinforced concrete to external forces, stresses transferred in concrete due to the interaction of the crack surfaces and longitudinal stresses in reinforcement are considered here. The constitutive laws for reinforcing steel and concrete cracks are assumed to be independent. It is further assumed, based on the assumption of infinitesimal deformation, that axial forces in reinforcing steel are always in the direction of the reinforcement axis before deformation. This assumption is equivalent to ignoring shear transfer in reinforcing steel (dowel action).

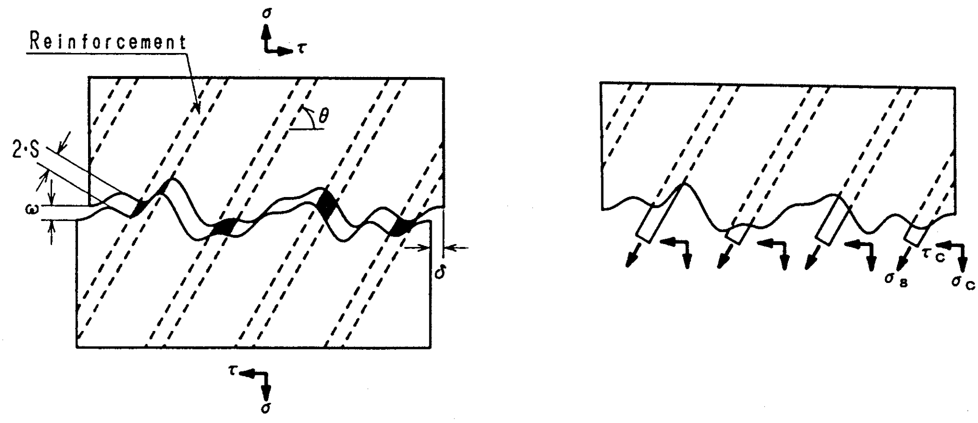

Fig.1 Discrete Crack

The discussion on the proposed model in this chapter deals only with discrete cracks in isotropically reinforced concrete. It is, however, easy to expand the model to make it applicable to cases where multiple reinforcing bars are laid in multiple directions, by assuming that the constitutive laws of each reinforcing bar are independent.

2.2 Stresses at discrete crack surfaces and their equilibrium

It can be considered, from the basic assumptions, that the stress $\{\sigma_j\} = [\tau, \sigma]^T$ along a discrete crack surface is the sum of the stress $\{\sigma_{jc}\}$ due to concrete and the stress $\{\sigma_{js}\}$ due to reinforcing steel. Thus,

$$\{\sigma_j\} = \{\sigma_{jc}\} + \{\sigma_{js}\} = [\tau_c, \sigma_c]^T + [\tau_s, \sigma_s]^T, \tag{1}$$

where τ : shear stress at discrete crack surface
σ : normal stress at discrete crack surface (tension=positive)
τ_c: shear stress in concrete
σ_c: normal stress in concrete (tension=positive)
τ_s: shear stress due to reinforcing steel
σ_s: normal stress due to reinforcing steel (tension=positive).

Since axial forces in reinforcing steel are in the direction of the reinforcement axis before deformation, if the reinforcement ratio (total sectional area of reinforcing steel passing through crack surface ÷ area of crack surface) for a crack surface is represented by p^* , the steel stresses τ_s and σ_s can be expressed as follows:

$$\tau_s = p^*\sigma_{as}\cos\theta \quad , \quad \sigma_s = p^*\sigma_{as}\sin\theta, \tag{2}$$

where σ_{as} is axial stress in reinforcing steel.

The relationship between the reinforcement ratios denoted by p for a section perpendicular to reinforcing steel and p^* can be expressed as follows:

$$p^* = p\sin\theta. \tag{3}$$

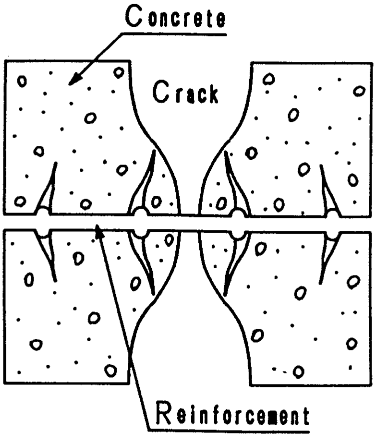

Fig.2 Width of Local Crack

From the above, the total stresses τ and σ can be calculated from the axial stress σ_{as} and the concrete stress τ_c,σ_c:

$$\tau = \tau_c + p\,\sigma_{as}\cos\theta\sin\theta \quad , \quad \sigma = \sigma_c + p\,\sigma_{as}\sin^2\theta. \tag{4}$$

2.3 Compatibility conditions for displacement

It is assumed that the displacement $\{u\}$ of a crack surface in reinforced concrete can be represented by the shear slip δ and the opening ω of the discrete crack:

$$\{u\} = [\delta, \omega]^T. \tag{5}$$

It is generally known that in cases where deformed bars are used for reinforcement, the widths of cracks near the reinforcing bars are very small and become larger as the distance from the bars increases. This means that the widths of local cracks in a section are not uniform (Fig.2)[8]. Since the model considered here is formulated on the basis of average behavior in a section, the opening ω of a discrete crack can be regarded as the average opening in the section.

In this study, steel stress is given as a function of the slip S of steel out of a discrete crack surface. To determine the steel stress $\{\sigma_{js}\}$ for the crack displacement $\{u\}$, therefore, it is necessary to determine the relationship between the steel slip S out of the crack surface and the discrete crack displacement $\{u\}$. By assuming that the steel slip S out of the crack surface equals half of the crack opening ω when reinforcement is perpendicular to the crack surface, the steel slip S out of the crack surface was defined, using the opening ω, as follows:

$$S = \omega/2. \tag{6}$$

It is estimated that in cases where reinforcing steel passes through a crack surface diagonally, the steel develops local shear deformation if displacement occurs. Nevertheless, because the crack width is sufficiently small as compared with the diameter of reinforcing steel, the steel in concrete can be considered to continue to act as a linear element after the occurrence of deformation. By ignoring the deformation of concrete, compatibility conditions for infinitesimal deformation shown below can be derived.

$$S = (\delta\cos\theta + \omega\sin\theta)/2. \tag{7}$$

If $\theta = \pi/2$ is substituted in Eq.(7), Eq.(7) becomes identical to Eq.(6) and hence the equation is applicable to orthogonal reinforcement.

2.4 Steel slip model

The steel slip model for discrete cracks considered in this study is based on the steel strain-slip models proposed by Shima et al.[4] and Shin et al.[3]. The model reflects bond deterioration of reinforcement in any direction and is designed to accurately express the behavior of reinforcing steel after being subjected to a high degree of plasticity under reversed cyclic loading. Since the details of the model will be given in Chapter 3, the procedure for calculating steel stress from the steel slip S out of the crack surface will be explained here. Hereafter S will be referred to as the steel slip for convenience.

The steel strain-slip model is formulated on the basis of the normalized steel slip denoted by s[4] which was derived by normalizing the steel slip S, considering the influences of steel diameter and concrete strength. Generally, the model can be expressed as a function of steel strain ε_s at the crack:

$$s = s(\varepsilon_s), \tag{8}$$

where $s = (S/D) \cdot K_{fc}$
$K_{fc} = (f'_c/20)^{\frac{2}{3}}$
D : diameter of reinforcing steel
f'_c : concrete compressive strength (MPa)
$s(\varepsilon_s)$: function reflecting the history of steel strain ε_s.

For the purposes of this study, Eq.(8) solved for s is used in the following form:

$$\varepsilon_s = \varepsilon_s(s). \tag{9}$$

Generally, the steel stress-strain relationship can be expressed as follows:

$$\sigma_{as} = \sigma_{as}(\varepsilon_s). \tag{10}$$

Steel stress σ_{as} , therefore, can be obtained by calculating the steel strain ε_s from the steel slip S by use of Eq.(9), and then using Eq.(10). Thus, the axial stress in reinforcing steel is a unique function of the steel slip s , and can be expressed as follows:

$$\sigma_{as} = F_s(s), \tag{11}$$

where $F_s(s)$ is a nonlinear function dependent on the history of the steel slip s. In this study, Kato's model[9] is used as the model of the steel stress-strain relationship. The accuracy of the model is not discussed here with the understanding that it has already been demonstrated.

2.5 Concrete model

(a) Before cracking

Assuming that concrete at a discrete crack surface before cracking behaves elastically, concrete stresses τ_c and σ_c at the discrete crack surface were defined as follows:

$$\left\{ \begin{array}{c} \tau_c \\ \sigma_c \end{array} \right\} = \left[\begin{array}{cc} G_c/\ell & 0 \\ 0 & E_c/\ell \end{array} \right] \left\{ \begin{array}{c} \delta \\ \omega \end{array} \right\}, \tag{12}$$

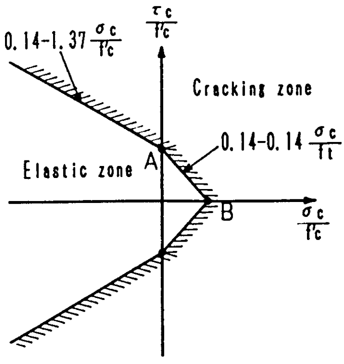

Fig.3 Cracking Conditions

where E_c : Young's modulus
G_c : shear modulus
ℓ : effective height of crack surface.

Generally, thickness is not considered in a discrete crack model. The effective height l of the crack surface, therefore, should be 0. However, if $\ell = 0$ is assumed, the stiffness term in Eq.(12) becomes infinite. Hence the effective height of the crack surface was represented by ℓ , and a value roughly corresponding to the maximum aggregate size for concrete was used for purposes of numerical analysis.

(b) Cracking conditions

It can be considered that while a discrete crack surface is purely in tension, that is, while only normal stress σ_c is applied, cracking occurs when σ_c has exceeded the tensile strength f_t of concrete. On the other hand, there are still many unknowns about cracking conditions under simultaneously applied shear stress and normal stress. This is particularly true in cases where a great compressive stress is being applied on a discrete crack surface.

In this study, the cracking conditions were expressed, on the basis of the results of the push-off test[10], on plain concrete specimens conducted by Lim et al., as follows (Fig.3):

$$\tau_c/f_c' = \begin{cases} 0.14 - 1.37\sigma_c/f_c' \\ 0.14 - 0.14\sigma_c/f_t \end{cases} . \tag{13}$$

Since Lim et al. did not refer to cases where tensile stress is applied on a discrete crack surface, the failure criterion for cases where normal stress is not applied on the discrete crack surface (Point A) and the one for cases where only tensile stress is applied on the discrete crack surface (Point B) were interpolated linearly, as shown in Fig.3.

Cracking was taken as having occurred when concrete stress calculated from Eq.(12) entered the shaded zone. Thereafter, a universal contact density model proposed by Bujadham et al., explained below, was used.

(c) After cracking

As a model of stress transfer at a surface of a crack in concrete after cracking, a model proposed by Bujadham et al., a generalized version of Li and Maekawa's contact surface density function[5], was used. The model expresses (1) friction and local plastic deformation at contact points on the crack surface, (2) progressive fracture at contact points, and (3) anisotropic plastic behavior at contact points individually in a highly generalized manner. For details of the model, see Reference [7].

The universal contact surface density model of Bujadham et al., like Li-Maekawa's model, is based on a contact density function, and the model has improved accuracy in deformation modes in which both the closing of cracks and shear slip occur. If the normal and tangential contact force densities of a unit crack element are represented by Z_n and Z_t, respectively, then concrete stresses τ_c and σ_c can be given, as functions of crack displacement δ and ω , as follows:

$$\begin{aligned}\tau_c &= \int_{-\pi/2}^{\pi/2}\{Z_n(\delta,\omega,\theta)\sin\theta + Z_t(\delta,\omega,\theta)\cos\theta)\}d\theta \\ \sigma_c &= \int_{-\pi/2}^{\pi/2}\{Z_n(\delta,\omega,\theta)\cos\theta - Z_t(\delta,\omega,\theta)\sin\theta)\}d\theta.\end{aligned} \tag{14}$$

If the normal contact stress and the tangential frictional stress of a unit crack element are represented by σ_{con} and τ_{fric} , the contact force densities Z_n and Z_t can be expressed as follows:

$$\begin{aligned}Z_n &= A_t\sigma_{con}(\delta,\omega,\theta)K(\omega)\Omega(\theta) \\ Z_t &= A_t\tau_{fric}(\delta,\omega,\theta)K(\omega)\Omega(\theta),\end{aligned} \tag{15}$$

where A_t : contact surface ratio
$K(\omega)$: contact ratio of crack surface
$\Omega(\theta)$: contact density function.

Since concrete stress in this model is given explicitly as a nonlinear function of crack displacement, tangential material matrices of stiffness are not necessary for stress evaluation. Tangential material matrices may be necessary, however, in obtaining an equilibrium solution. For example, when the crack displacement corresponding to a given stress is to be calculated, tangential material matrices may be needed to obtain an equilibrium solution through iterative calculation. If the convergence of the solution is guaranteed, tangential matrices do not need to be exact[11]. Since the differentiation in Eq.(14) is very complicated, for purposes of this study, the following approximate tangential material matrix was used in nonlinear iterative calculation:

$$\begin{aligned}D_{11} &= \int_{-\pi/2}^{\pi/2} A_tK(\omega)(E_{ct}\sin^2\theta - G_{ct}\cos^2\theta)\Omega(\theta)d\theta \\ D_{12} &= \int_{-\pi/2}^{\pi/2} A_tK(\omega)(E_{ct}\cos^2\theta + G_{ct}\cos\theta\sin\theta)\Omega(\theta)d\theta \\ D_{22} &= \int_{-\pi/2}^{\pi/2} A_tK(\omega)(E_{ct}\cos^2\theta + G_{ct}\sin^2\theta)\Omega(\theta)d\theta \\ D_{21} &= D_{12},\end{aligned} \tag{16}$$

where $D_{11} = d\tau_c/d\delta$, $D_{12} = d\tau_c/d\omega$
$D_{21} = d\sigma_c/d\delta$, $D_{22} = d\sigma_c/d\omega$
E_{ct} : tangential stiffness (material constant) of individual fine crack element in the normal direction
G_{ct} : tangential stiffness (material constant) of individual fine crack element in the tangential direction.

2.6 Material matrices for reinforced concrete discrete cracks

Since the material models used are nonlinear, it is necessary to use repeated calculation to obtain solutions. The basic constitutive equations in the incremental form are given below.

The reinforcement model can be written, in the incremental form, as follows:

$$d\sigma_{as} = D_s dS, \tag{17}$$

where $D_s = (dF_s/ds) \cdot K_{fc}/D$. Substituting the incremental form of Eq.(7) in Eq.(17) and expressing it in matrix representation using Eq.(2), we obtain

$$\{d\sigma_{js}\} = pD_s \sin\theta/2 \cdot [R(\theta)]^T [R(\theta)]\{du\} = [D_{js}]\{du\}, \tag{18}$$

where $[R(\theta)] = [\cos\theta, \sin\theta]$. The incremental form of the concrete model can be written as

$$\begin{aligned} d\tau_c &= D_{11} d\delta + D_{12} d\omega \\ d\sigma_c &= D_{21} d\delta + D_{22} d\omega. \end{aligned} \tag{19}$$

Expressing the above equation in matrix representation, we have

$$\{d\sigma_{jc}\} = [D_{jc}]\{du\}. \tag{20}$$

By substituting Eq.(18) and Eq.(20) in the incremental form of Eq.(1), the following constitutive equation for discrete cracks is obtained:

$$\{d\sigma_j\} = [D_j]\{du\}, \tag{21}$$

where $[D_j] = [D_{jc}] + [D_{js}]$. Since $[D_j]$ can be considered to be a tangential material matrix for discrete cracks, it can be represented by components as follows:

$$[D_j] = \begin{bmatrix} D_{11} + pD_s \cos^2\theta \sin\theta/2 & D_{12} + pD_s \cos\theta \sin^2\theta/2 \\ D_{21} + pD_s \cos\theta \sin^2\theta/2 & D_{22} + pD_s \sin^3\theta/2 \end{bmatrix}. \tag{22}$$

3 GENERALIZED STEEL MODEL FOR DISCRETE CRACK IDEALIZATION

The steel slip model employed here is based on the steel strain-slip model[4] proposed by Shima et al.. However, their model was derived on the basis of an experiment conducted under ideal conditions (for example, the possibility of the occurrence of a splitting crack in concrete at the loading end is minimized). In this study, we are going to carry out a test of RC plates subjected to reversed cyclic loading and to reconstruct a steel model based upon the experimental results.

3.1 Test of RC plates

(a) Specimens and test conditions

As shown in Fig.4, the specimens used in the test are reinforced concrete plates, (thickness: 100 mm) each of which has a 1,000-mm-long, through-depth crack running through the center of the plate in the direction perpendicular to the axis of loading. The notch running through the center of the specimen is intended to limit the location of the crack. The crack, which is induced by the notch, is the object of measurement. As shown, each specimen is provided with another set of notches 150 mm from the center line of the specimen. The purpose of this arrangement is to ensure an adequate stiffness of the crack region, thereby achieving consistent measuring accuracy.

In each plate specimen, two layers of reinforcing bars are arranged in orthogonal directions. The angle between the test crack surface and the direction of reinforcement is a major parameter here. Outside the test zone are anchoring zones with slits. Specifications and test conditions used are shown in Tables 1 and 2.

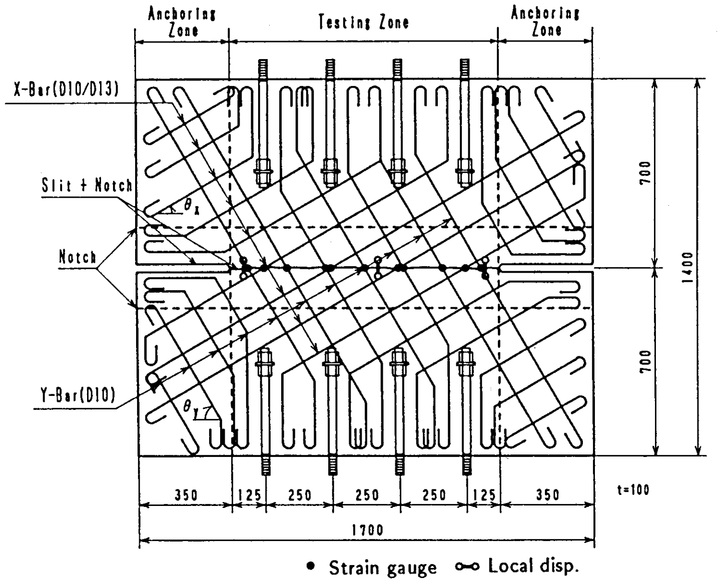

Fig.4 Reinforced Concrete Plate Specimen (unit:mm)

Table 1 Specimens

Name	Concrete compressive strength (MPa)	X-steel bar			Y-steel bar		
		Steel diameter	Angle (deg.)	Reinf. ratio (%)	Steel diameter	Angle (deg.)	Reinf. ratio (%)
No.1	37.6	D10	90	1.1	D10	0	1.14
No.2	40.4	D10	45	1.1	D10	45	1.14
No.3	38.6	D10	30	1.1	D10	60	1.14
No.4	39.2	D13	45	2.0	D10	45	1.14
No.5	24.5	D10	30	1.1	D10	60	1.14
No.6	26.2	D13	45	2.0	D10	45	1.14

Table 2 Mechanical Properties of Reinforcing Steel

	No.1-4		No.5,6	
	D10	D13	D10	D13
Yield stress (MPa)	403	409	414	429
Young modulus(GPa)	183	197	192	200
Strength (MPa)	536	561	550	562

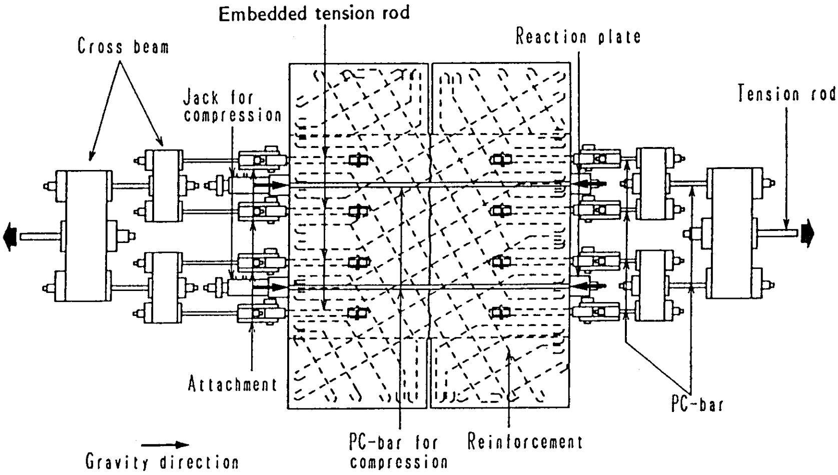

Fig.5 Loading Method

(b) Loading and measuring method

Uniaxial reversed cyclic loads were applied to the specimen in the direction perpendicular to the cracking direction (Fig.5). In the loading, stresses occurring in concrete near the crack as well as in reinforcing steel were varied by using different angles of reinforcement in the specimen. Jacks on independent hydraulic systems were installed on the tension side and the compression side, and the hydraulic systems were switched during reversed cyclic loading according to the direction of loading. The tournament method[12] adopted by Aoyagi and Yamada was used in tensile loading. Four jacks were used in compressive loading, and the hydraulic pipes for the jacks were arranged serially so that the jacks produced equal loads, thereby applying uniform in-plane stresses to the specimen.

Strain gauges were attached to all reinforcing bars encompassing the test cross section of the specimen so that stresses in the reinforcing steel and concrete along the test cross section could be distributed accurately (Fig.4). Slip displacement and opening displacement at the crack were measured with noncontact-type precision displacement gauges installed on the test cross section of the specimen at an interval of 50 mm (Fig.4). Measurements taken at three points each on both sides of the specimen were averaged to obtain the relative displacement at the test cross section.

3.2 Steel strain-slip model for monotonic loading

(a) Reinforcement perpendicular to crack

Figure 6 illustrates the steel strain-slip relationship for Specimen No.1 before yielding of reinforcing steel. The figure also shows Shima's model for purposes of comparison. It shows that the slip of reinforcing steel in Specimen No.1 is considerably greater than the slip value corresponding to the same strain value based on the Shima's model.

When reinforcing steel passes through a crack surface in reinforced concrete, bond deterioration near the crack surface is inevitable[13]. It is therefore necessary to consider its influence in modeling the strain-slip relationship for reinforcing steel. Shin defined bond deterioration zones as 5D zones from the crack surface and assumed that bond distribution in these zones is linear. Shin's model is actually an expansion of the Shima's model. The Shin model agrees well with test results for Specimen No.1. It can be considered that under the test conditions employed here, the lengths of bond deterioration zones remain constant regardless of strains in reinforcement. The model used for monotonic loading is shown in Fig.7.

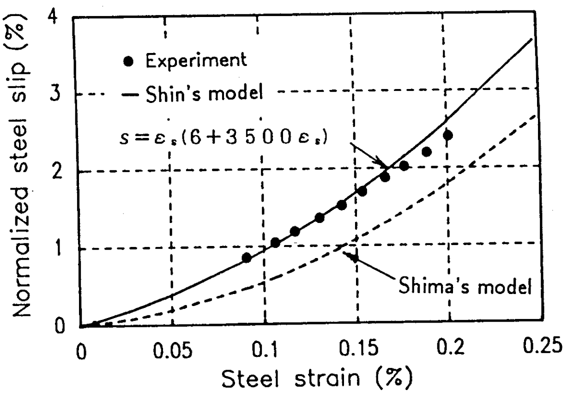

Fig.6 Steel Strain-Slip Relationship before Yielding

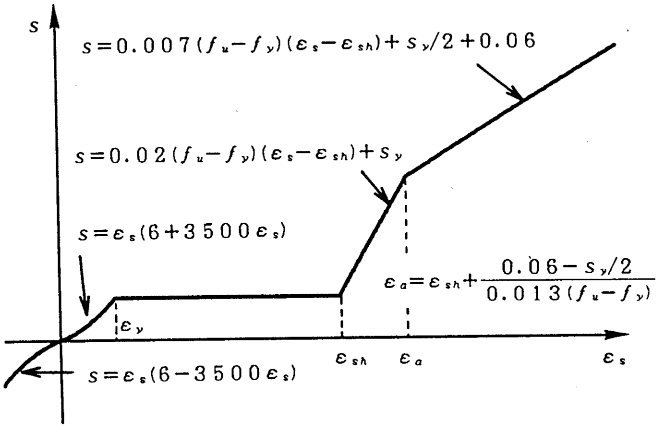

Fig.7 Steel Strain-Slip Model for Monotonic Loading

Niwa et al. pointed out that a steel strain-slip model for the monotonic compressive loading of reinforcing steel should differ from a steel strain-slip model for tensile loading[14]. Factors affecting this are thought to include the relationship between the bleeding direction and the reinforcement axis direction, settlement of concrete, and Poisson's ratio for reinforcing steel in compression. In cases where compression is fully transferred through a surface of concrete, reinforcing steel at a discrete crack in a reinforced concrete member is rarely loaded monotonically. For the purpose of simplification of the model, therefore, it was assumed that bond characteristics under monotonic loading on the compression side and the tension side are identical, and similar steel strain-slip models were used for positive and negative loading.

(b) Reinforcement diagonal to crack

As mentioned earlier, when orthogonal reinforcement is considered, the influence of bond deterioration near the crack surface cannot be ignored. In the case of diagonal reinforcement, too, local failure is likely to occur in concrete near the crack surface. Figure 8 is a plot of the relationship between the normalized steel slip s $(= S/D \cdot K_{fc})$ for the reinforcing steel in each specimen obtainable from the steel slip S, which can be calculated from Eq.(7), and the steel strain ε_s at the crack within the steel's elastic range. The relationship was plotted in order to evaluate the influence of the angle of reinforcement θ and the relative displacement δ_s in the direction perpendicular to the reinforcement on the steel strain-slip relationship. As shown, the plot roughly follows Shin's model for perpendicular reinforcement though there are some variations among the reinforcing bars. These data show no

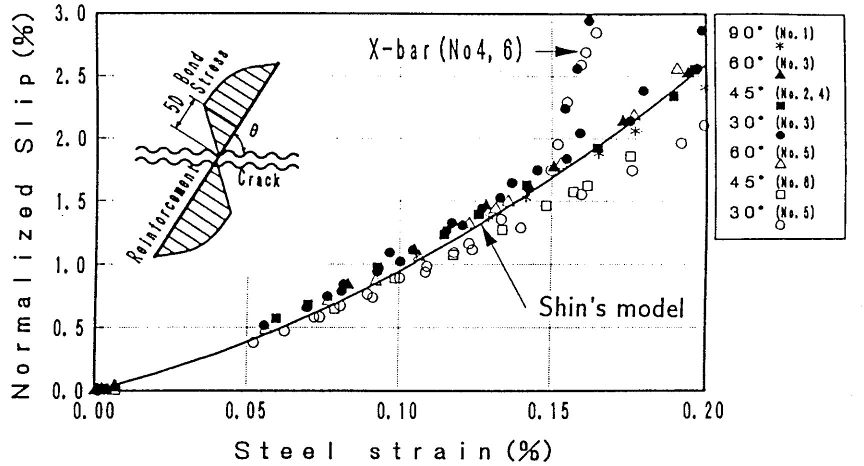

Fig.8 Steel Strain-Slip Relationship of Each Bar

significant influence of θ or δ_s on slip characteristics. The fact that Fig.8 includes data on the low-strength specimens (No.5 and 6) indicates that the influence of concrete strength can be evaluated by means of K_{fc} . Figure 8 shows the relationship between the normalized steel slip and the steel strain at and after yielding of reinforcing steel. Like the relationship before yielding of reinforcing steel, the relationship shown here agrees well with the Shin's model for all reinforcing bars considered.

From the above, it can be concluded that under the test conditions employed here the bond deterioration zones can be defined as the 5D zones along the reinforcing steel, regardless of the angle of steel and the relative displacement at the crack surface.

3.3 Reversed cyclic model of reinforcement before yielding

Figure 9 shows the steel strain-slip relationship for Specimen No.1 before yielding of reinforcing steel. Calculated values shown in the figure were obtained from the model proposed by Shin[3]. As shown, the calculated relationship before yielding of reinforcing steel agrees well with Shin's model. Hence, the model is used here without modification. The cyclic model is shown in Fig.10.

3.4 Cyclic model of reinforcement after yielding

Figure 11 shows the steel strain-slip relationship after yielding of reinforcement. Note that strain in the reinforcing steel subjected to a tensile deformation of up to about 30,000 μ (when all reinforcing bars are thought to be in the strain hardening range) recovers to about 5,000 μ after compressive loading. This means that the reinforcing bars do act as compression members during compressive loading. This is therefore an important check item in modeling the steel strain-slip relationship after yielding of reinforcement. Shin uses the same cyclic model for both preyielding and postyielding behavior. Although the behavior during unloading on reinforcing steel that has undergone high plasticity is expressed consistently by the Shin's model, the model leaves room for improvement in ranges in which "slip back" predominates. In this section, this highly plastic region is highlighted, and an attempt will be made to expand the applicability of the Shin's model so as to construct a generalized discrete crack model.

(a) Modeling concept

As shown in Fig.12, the distribution of steel strain after yielding of reinforcing steel is thought to be discontinuous at the boundary of the steel yield region and the elastic region (yield boundary point). This suggests that in order to define the relationship between steel strain and steel slip after yielding of reinforcement, it is more reasonable to model the relationship in the steel yield region and the elastic region separately. Here steel strain in the cracking section, strain on the yield region side of the

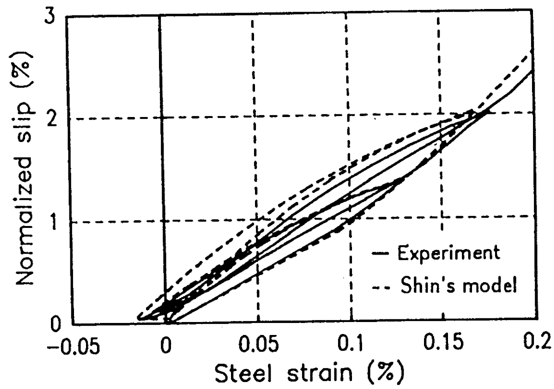

Fig.9 Steel Strain-Slip Relationship for Cyclic Loading (Before Yielding)

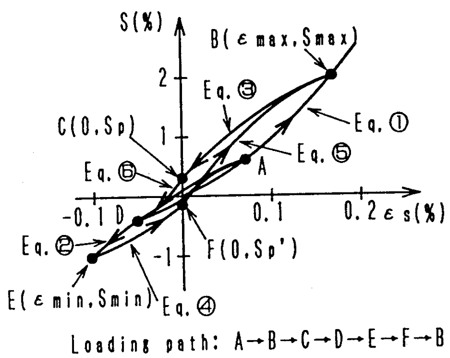

① $s=\varepsilon_s(6+3500\varepsilon_s)$, ② $s=\varepsilon_s(6-3500\varepsilon_s)$

③ $s=s_{max}-\varepsilon'_s(6+3500\varepsilon'_s)\cdot 0.85,\ \varepsilon'_s=\varepsilon_{max}-\varepsilon_s$

④ $s=s_{min}-\varepsilon''_s(6-3500\varepsilon''_s)\cdot 0.85,\ \varepsilon''_s=\varepsilon_{min}-\varepsilon_s$

⑤ $s=0.6(s'_p-s_{max})/\varepsilon_{max}{}^2\cdot(\varepsilon_s-4/3\cdot\varepsilon_{max})^2 + (16s_{max}-s'_p)/15$

⑥ $s=0.6(s_p-s_{min})/\varepsilon_{min}{}^2\cdot(\varepsilon_s-4/3\cdot\varepsilon_{min})^2 + (16s_{min}-s_p)/15$

Fig.10 Steel Strain-Slip Model for Cyclic Loading (Before Yielding)

yield boundary point, and strain on the elastic region side are defined as ε_s, ε_{sp} and ε_{se}, respectively. Similarly, steel stresses are defined as σ_{as}, σ_{sp} and σ_{se} .

It is assumed that the normalized steel slip s can be expressed as the sum of the slip s_{pl} in the yield region and the slip s_e in the elastic region.

$$s = s_{pl} + s_e. \tag{23}$$

The slip s_{pl} and s_e are modeled separately below.

(b) Modeling the yield region

If the deformation of concrete is ignored, the steel slip can be defined as the steel strain integrated along the reinforcement axis. If the distribution of strain in the yield region is assumed to be linear, the normalized steel slip s_{pl} can be expressed as follows:

$$s_{pl} = \frac{\varepsilon_s + \varepsilon_{sh}}{2} \cdot \ell_y \cdot (K_{fc}/D), \tag{24}$$

where ℓ_y is the length of the yield region from the crack. It is assumed that the yield region expands only when a new loading cycle begins, and it does not change during unloading or reloading.

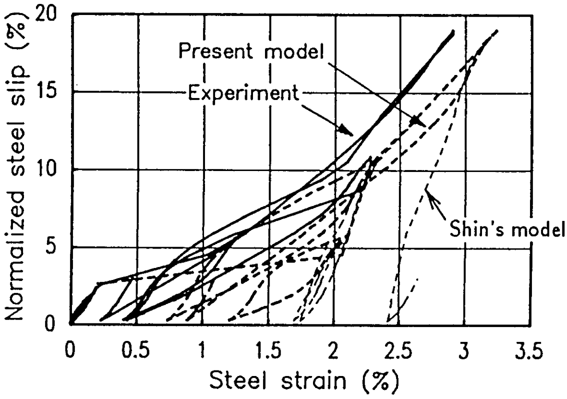

Fig.11 Steel Stress-Slip Relationship for Specimen No.1

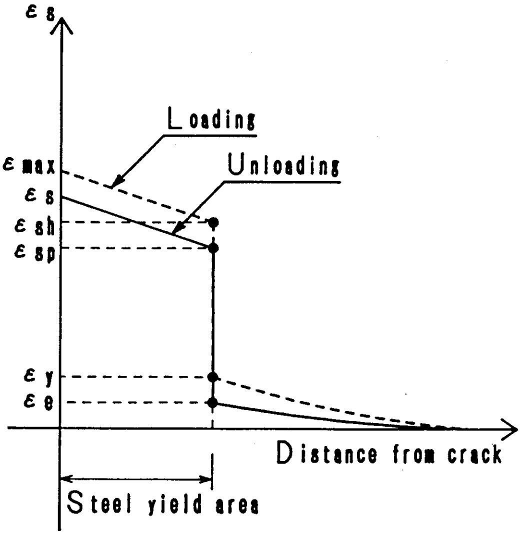

Fig.12 Distribution of Strain along the Reinforcement Bar (After Yielding)

Ideguti et al. pointed out[15] that the strain ε_s at the yield boundary point during unloading and reloading is almost univocally related with the strain ε_{sp} at the crack surface (Fig.13). In this study, this relationship is considered and the following relationship between ε_s and ε_{sp} is assumed:

$$\varepsilon_{sp} = \varepsilon_{sh} - \beta(\varepsilon_{max} - \varepsilon_s), \tag{25}$$

where β is a parameter representing the gradient of the line shown in the figure, and $\beta \approx 1.0$. Here, this parameter is regarded as a material parameter. By substituting Eq.(25) into Eq.(24), we obtain

$$s_{pl} = \frac{(1+\beta)\varepsilon_s + \varepsilon_{sh} - \beta\varepsilon_{max}}{2} \cdot \ell_y \cdot (K_{fc}/D). \tag{26}$$

If Kato's model[9] is applied to the steel stress-strain relationship in the yield boundary region, the steel stress σ_{sp} can be calculated from the steel strain ε_{sp} (Fig.14). Thus, the steel stress can be given as follows:

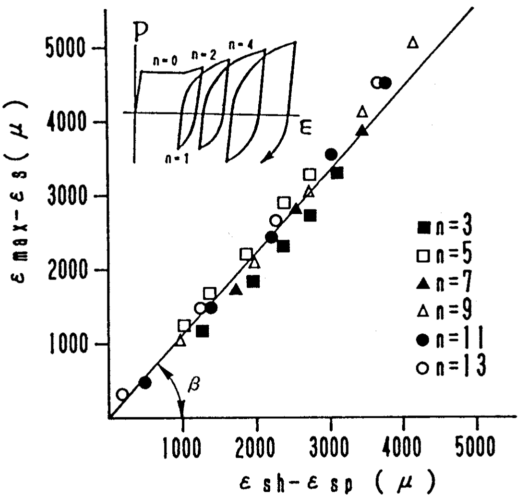

Fig.13 Relationship between ε_s and ε_{sp}

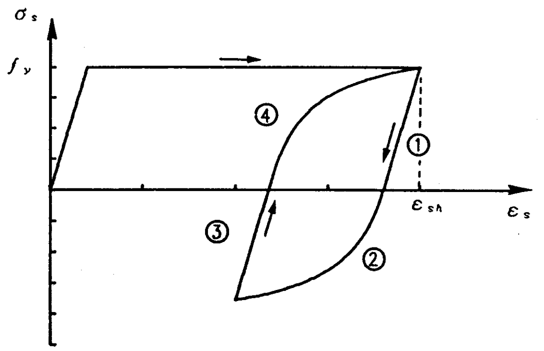

Fig.14 Steel Strain-Slip Model (Kato's model)

1) During unloading (① in Fig.14)

$$\sigma_{sp} = \sigma_y - E_s(\varepsilon_{sh} - \varepsilon_{sp}) \tag{27}$$

2) During negative loading (②)

$$\sigma_{sp} = -f_y \left[a - \frac{a(a-1)}{-\left(\frac{E_B}{f_y}\right)(\varepsilon_{sp} - \varepsilon_{sh} + \varepsilon_y) + a - 1} \right], \tag{28}$$

where $E_B = -(E_s/6) \cdot \log_{10} 10(\varepsilon_{sh} - \varepsilon_y)$, $a = E_s/(E_s - E_B)$

3) During re-unloading (③)

$$\sigma_{sp} = \sigma_{pm} + E_s(\varepsilon_{sp} - \varepsilon_{pm}), \tag{29}$$

where σ_{pm} : minimum value of σ_{sp} in the loading history

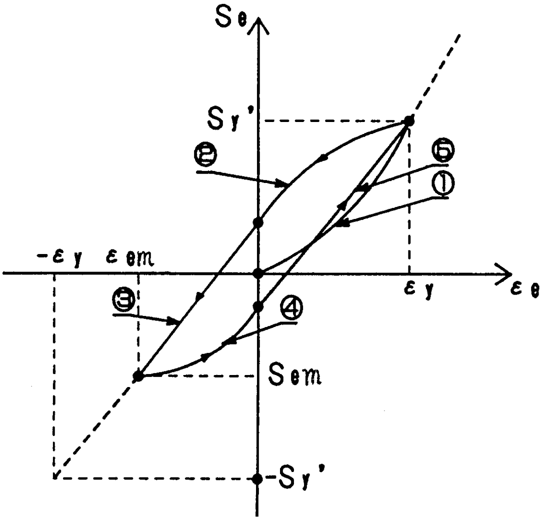

Fig.15 Simplified Shima Model

ε_{pm} : minimum value of ε_{sp} in the loading history

4) During reloading (④)

$$\sigma_{sp} = \sigma_y + \sigma_{pm} + f_y \left[a - \frac{a(a-1)}{-\left(\frac{E_B}{f_y}\right)(\varepsilon_y - \varepsilon_{sp} + \varepsilon_{pm}) + a - 1} \right]. \tag{30}$$

(c) Modeling the elastic region

It is assumed that a hysteresis obtained by simplifying Shima's basic model[4], as shown in Fig.15, is applicable to the relationship between the steel strain ε_{se} and the steel slip s_e in the elastic region. Since the elastic section of reinforcing steel is rather distant from the crack surface, it was assumed that the influence of bond deterioration does not reach the elastic boundary point. Thus, the following equations can be derived from the Shima's model.

1) During unloading (②)

$$s_e = s_y^* - 0.85(\varepsilon_y - \varepsilon_{se})(2 + 3500(\varepsilon_y - \varepsilon_{se})), \tag{31}$$

where $s_y^* = \varepsilon_y(2 + 3500\varepsilon_y)$

2) During negative loading (③)

$$s_e = 0.15 s_y^* + 1.15 \frac{s_y^*}{\varepsilon_y} \cdot \varepsilon_{se} \tag{32}$$

3) During re-unloading (④)

$$s_e = s_{em} + 0.85(\varepsilon_e - \varepsilon_{em})(2 + 3500(\varepsilon_e - \varepsilon_{em})), \tag{33}$$

where s_{em} : minimum value of s_e in the loading history
ε_{em} : minimum value of ε_{se} in the loading history

4) During reloading (⑤)

$$s_e = s_{ep} + \frac{s_y^* - s_{ep}}{\varepsilon_y} \cdot \varepsilon_e, \tag{34}$$

where $s_{ep} = s_{em} - 0.85\varepsilon_{em}(2 - 3500\varepsilon_{em})$.

Generally, the steel stress-strain relationship after yielding of reinforcing steel shows discontinuity. Hence the steel strain distribution may be discontinuous, but the steel stress distribution does not become discontinuous. Therefore, considering the continuity of the steel stress, $\sigma_{se} = \sigma_{sp}$,

$$\varepsilon_{se} = \sigma_{sp}/E_s. \tag{35}$$

Thus, ε_{se} can be calculated from ε_{sp}, using Eqs.(27) to (30). This means, considering Eq.(25) and Eqs.(31) to (34), that the steel slip s_e has now been given as a function of the steel strain ε_s at the crack surface.

(d)Length of the yield section

Now that the slips s_e and s_{pl} for a given history of the steel strain ε_s have been formulated, it is possible to calculate the steel slip s by totaling steel slips in the elastic region and the plastic region using Eq.(23). Then, the length of the yield section ℓ_y can be obtained as follows. If the steel slip immediately after the transition from loading to unloading is represented by s_u , then, by assuming $\varepsilon_s = \varepsilon_{max}$, we have,

$$s_u = \ell_y \cdot (K_{fc}/D) \cdot \frac{\varepsilon_{max} + \varepsilon_{sh}}{2} \cdot (s_{max} - s_y^*) + s_y^*. \tag{36}$$

To achieve the continuity of the model, the steel slip immediately after the transition to unloading must be equal to the steel slip before unloading. Hence, $s_u = s_{max}$. Solving Eq.(36) for ℓ_y , we obtain

$$\ell_y = 2\frac{s_{max} - s_y^*}{\varepsilon_{max} - \varepsilon_{sh}} \cdot (D/K_{fc}). \tag{37}$$

Since the Shin's model gives smax as a function of ε_{max} , the length ℓ_y of the yield section can be calculated from ε_{max} . By substituting Eq.(37) in Eq.(26), the steel slip s_{pl} can be given as follows:

$$s_{pl} = \frac{(1+\beta)\varepsilon_s + \varepsilon_{sh} - \beta\varepsilon_{max}}{\varepsilon_{max} + \varepsilon_{sh}} \cdot (s_{max} - s_y^*). \tag{38}$$

Although β takes a value of about 1.0 as mentioned earlier, it has been found that it is a preferable way to treat β as a function of stress history if a better agreement with the results of the reinforced concrete plate test described in 3.1 is to be achieved. In this study, β is calculated using the following equation:

$$\beta = \sigma_{max}/\sigma_y, \tag{39}$$

where σ_{max} is the maximum stress in reinforcement steel under tensile loads.

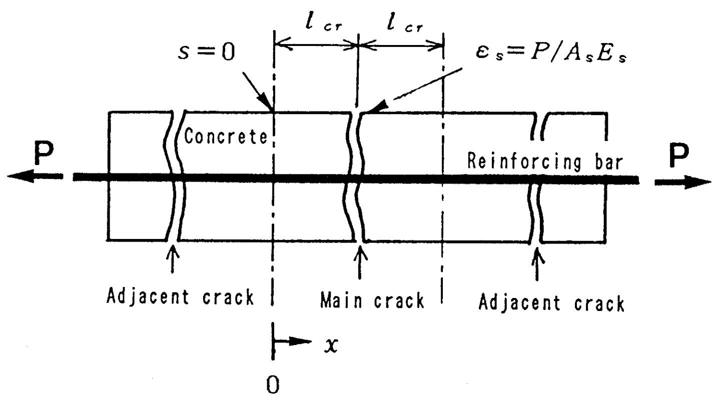

Fig.16 Uniaxial Reinforced Concrete Member in Tension

3.5 Model of interference of adjacent cracks

If the state of stress around a discrete crack surface is close to uniform and distances from adjacent cracks are small, then the influence of adjacent cracks cannot be ignored. In this section, interference of adjacent cracks is investigated through parameter analysis using the steel strain-slip-bond stress relationship[4] proposed by Shima et al.

If the distance between a main crack and an adjacent crack is defined as $2\ell_{cr}$ assuming a case where the tensile load P (in the elastic range) is applied on a crack surface, as shown in Fig.16, the following boundary conditions for bond hold:

$$s = 0 \qquad at \quad x = 0 \tag{40}$$

$$\varepsilon_s = P/(A_s E_s) \qquad at \quad x = \ell_{cr}, \tag{41}$$

where A_s : sectional area of reinforcing steel
E_s : elastic modulus of reinforcing steel.

The steel strain-slip relationship under monotonic loading in cases where there is a second crack near a main crack can be determined analytically by solving the basic equations for the bond under the above conditions using the steel strain-slip-bond stress relationship of Shima et al. as the constitutive law for the bond of reinforcement. Monotonic loading before and during yielding of reinforcement was analyzed using the steel diameter D and the crack interval $2\ell_{cr}$ as parameters, and the result of the analysis was compared with a model corresponding to the case where anchorage is sufficiently long, that is, the Shin's model. The comparison revealed that the influence of adjacent cracks can be approximately expressed by introducing a reduction factor $\alpha(\ell_{cr})$ that does not depend on steel strain (Fig.17). Then, the steel slip s_{cr} under monotonic loading that reflects the influence of adjacent cracks can be expressed as follows:

$$s_{cr} = \alpha \cdot s = \alpha \cdot (S/D) \cdot K_{fc}, \tag{42}$$

where $\alpha = 1 - \exp(-(0.0065\ell_{cr}/D + 0.5)^3)$ and $\alpha \leq 0.087\ell_{cr}/D$.

The crack interval $\ell_{cr}(\theta)$ in the case where reinforcing steel and the cracks cross diagonally is equal to a distance obtainable by converting the crack interval ℓ_{cr} for the direction of reinforcing steel. That is,

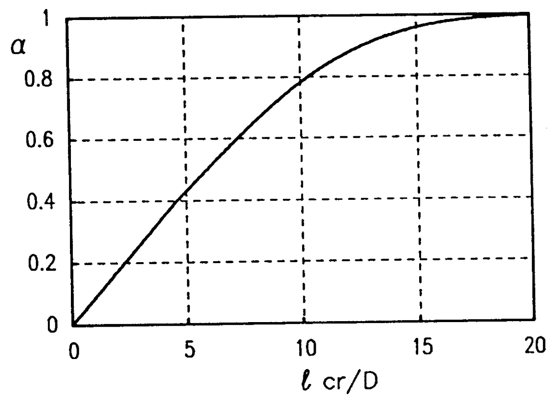

Fig.17 Relationship between Reduction Factor α and Crack Interval

$$\ell_{cr}(\theta) = \ell_{cr} / \sin\theta. \tag{43}$$

In analyses based on discrete crack models, the locations of discrete cracks are determined prior to discretization. In this study, therefore, ℓ_{cr} is treated as a given condition. Prediction of the crack interval is important in discrete crack models are to be used more reasonably. This is a problem yet to be addressed.

3.6 Comparison with experiments

Figure 11 compares the proposed model with test results for a plate specimen (No.1) with orthogonal reinforcement. Although even this model shows some difference from the test results, comparison with the Shin's model reveals that the proposed model is more accurate than the Shin's model in expressing strain-slip relationship during compression after yielding of reinforcing steel. Figure 18 shows the steel strain-stress relationship for the same specimen. As shown, test results and calculated values agree well throughout the loading process, indicating that the above-mentioned difference in steel strain can be ignored.

Figure 19 shows the relationships between opening displacement and steel stress in the case where reinforcing steel passes a crack surface diagonally (Specimen No.2). Test results and calculated values show good agreement, indicating that the proposed model is accurate enough to be applied to diagonal reinforcement. The compatibility condition for deformation, that is, Eq.(7), is used to calculate steel stresses from opening displacement. This means that Eq.(7) can be applied to the loading history considered here. In the above verification, it is assumed that the width of a crack as measured on the surface between reference points 50 mm apart is equal to the average width of the crack along the crack section.

4 VERIFICATION USING RC PLATES WITH SINGLE CRACK

In this chapter, the discrete crack model will be verified using the No.3 and 4 specimens.

4.1 Relationship between normal stress and crack opening

Figures 20 and Figure 21 compare the relationship between normal stress and crack opening determined through calculation with corresponding test results. Note here that crack opening was measured along the surface. The loading, unloading and reloading curves for each specimen obtained through analysis and testing agreed well, indicating that the proposed analytical model has sufficient accuracy.

Both the test results and the analysis showed that during compressive loading stiffness tended to increase under the influence of recontact of the crack surfaces. It depends greatly on the accuracy

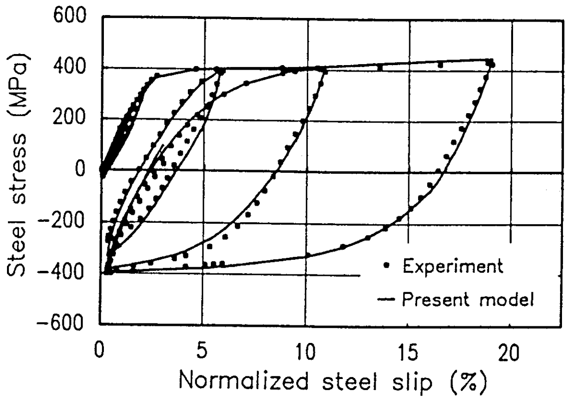

Fig.18 Steel Stress-Slip Relationship for Specimen No.1

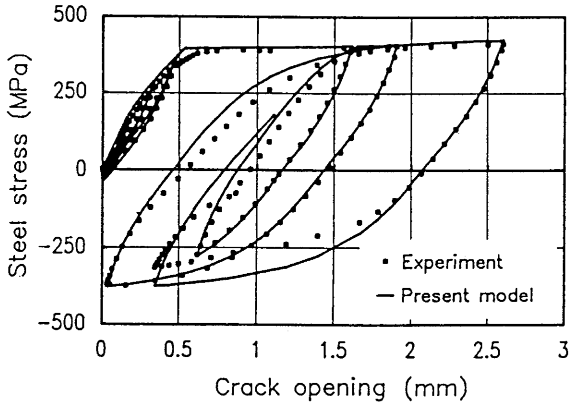

Fig.19 Steel Stress-Slip Relationship for Specimen No.2

of Bujadham's stress transfer model[7]. It is to be noted, however, that the displacement at which recontact begins as obtained from the analysis differs slightly from the one based on the test results. In order to improve accuracy further, it is necessary to improve the accuracy of the model in dealing with the path-dependent recontact of crack surfaces.

4.2 Relationship between crack opening and shear slip

Figure 22 illustrates the relationship between crack opening and shear slip. As shown, little shear slip occurred in Specimen No.3 even after yielding of reinforcing steel. Except when the crack surfaces are in recontact, concrete stresses are much smaller than steel stresses. This indicates that the behavior of Specimen No.3 is governed largely by the slip characteristics of reinforcing steel. Therefore, close agreement between the measured values and the calculated values shows the validity of the reinforcement model when applied to cyclic loading.

In Specimen No.4, by contrast, a shear slip roughly corresponding to crack opening occurred after yielding of reinforcing steel, and concrete stresses due to shear transfer occurred. The fact that the results of calculation for Specimen No.4 agree well with the results of the reversed cyclic loading test validates the concrete stress transfer model, too. Displacement at the crack surface after yielding of Y-steel is almost perpendicular to X-steel. Equation (7) suggests that little slip of X-steel occurred

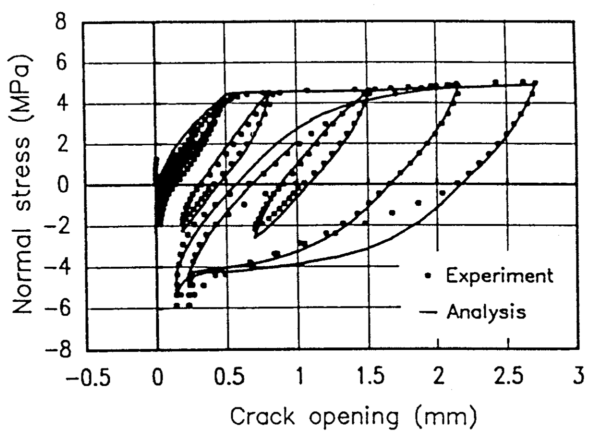

Fig.20 Relationship between σ and ω of Specimen No.3

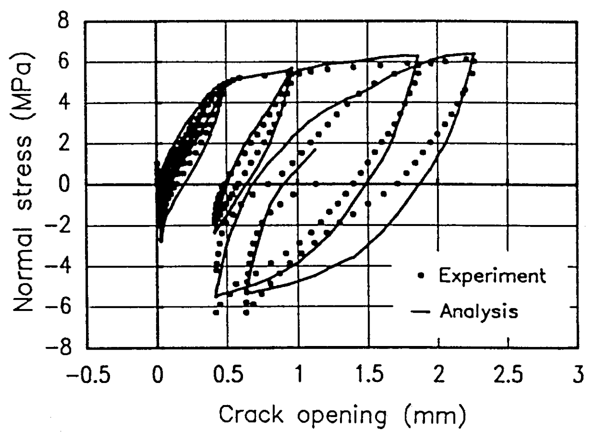

Fig.21 Relationship between σ and ω of Specimen No.4

after yielding of Y-steel.

4.3 Steel stress

Figures 23 and 24 show stresses in X-steel and Y-steel in Specimen No.4. X-steel did not yield because the displacement at the crack surface after yielding of Y-steel was almost perpendicular to X-steel, as mentioned in the preceding section. As shown, the analysis closely follows the test results, including this phenomenon.

4.4 Concrete stress transferred along crack surface

In reinforced concrete with anisotropic reinforcement, concrete stress occurs after the opening of a crack by the mechanism of stress transfer along the crack surfaces. Figure 25 compares the calculated and measured concrete stresses in Specimen No.4. The fact that small differences in crack opening are reflected in the calculated stresses indicates that the measured values and the calculated values agree well though the hysteresis curves are slightly different. Judging from the ratios of stresses transferred in concrete to stresses occurring along the crack surfaces, it can be concluded that the model has sufficient accuracy.

This verification depends largely on the steel slip model as part of the discrete crack model, and the

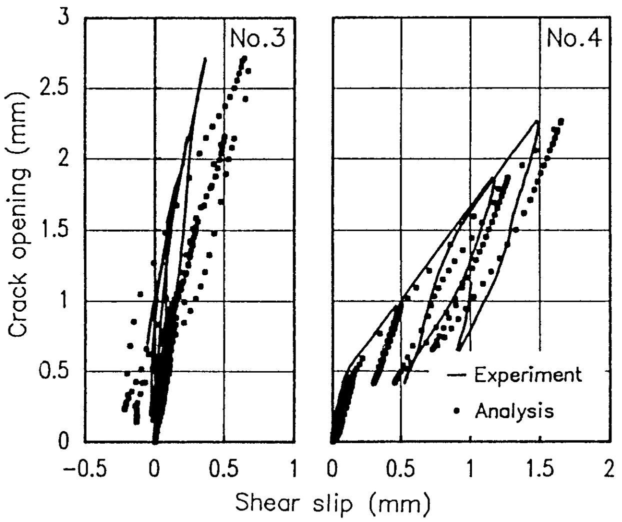

Fig.22 Relationship between ω and δ

concrete stress transfer model is not a major contributor to nonlinearity. It is therefore necessary to further evaluate applicability to discrete cracks involving the occurrence of high stresses along crack surfaces. This will be discussed in the next section.

5 VERIFICATION FOR SHEAR STRENGTH

In this section, the applicability of each model and strength prediction under high shear deformation will be considered through comparison with the results of a single shear test on reinforced concrete members.

5.1 Orthogonal reinforcement

A total of 59 specimens were chosen from the specimens, which have reinforcement perpendicular to the shear plane, based on the test data presented by Mattock and Hawkins[16] and Yamada and Aoyagi[17] These specimens were analyzed and their maximum shear strengths were compared. Results of the analysis are shown in Table 3. Figure 26 is a plot of the results, where the axis of abscissas represents the measured value and the axis of ordinates represents the calculated value. As a result, the ratio of the calculated value to the measured value of the maximum shear strength averaged 1.26, and the coefficient of variation, 13.7% . The difference between the calculated values and the measured values tended to increase with the increase in shear strength. This is due to the analytical model's inability to characterize the shear failure mode accurately for large reinforcement ratio.

In Fig.26, specimens whose reinforcement yielded in the analysis (steel yield failure mode) and those whose reinforcement did not yield even when the shear slip reached 3 mm (shear slip failure mode) are plotted separately. As shown, the analysis tends to give slightly higher values of shear strength even in the steel yield failure mode. Particularly, the calculated values based on the test data provided by Mattock and Hawkins are substantially greater than the observed values. Since the specimens Mattock and Hawkins used were smaller than those Yamada and Aoyagi used, weaker anchorage might be the cause of this tendency. Details were not known, however, it was assumed in the analysis that all reinforcing bars were anchored perfectly. Agreement with the test data provided by Yamada and Aoyagi was fairly good, except in the shear slip failure mode. The ratio of the calculated value to the measured value for the steel yield failure mode specimens of Yamada and Aoyagi averaged 1.09, and the coefficient of variation, 9.2% .

From the above, it has been confirmed that the model is accurate in the steel yield failure mode and

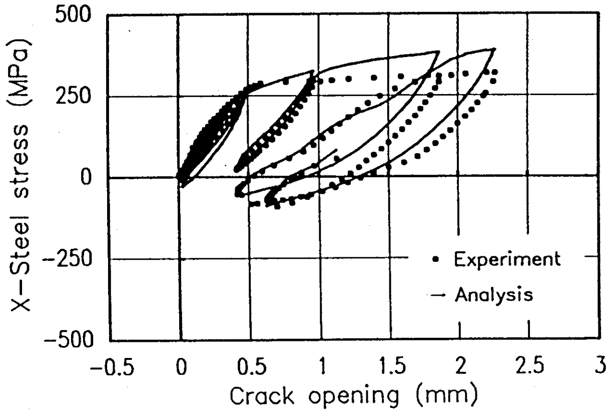

Fig.23 Steel Stress(X-Bar)

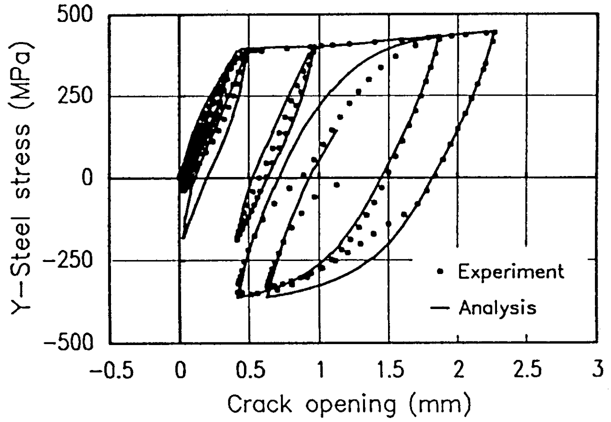

Fig.24 Steel Stress(Y-Bar)

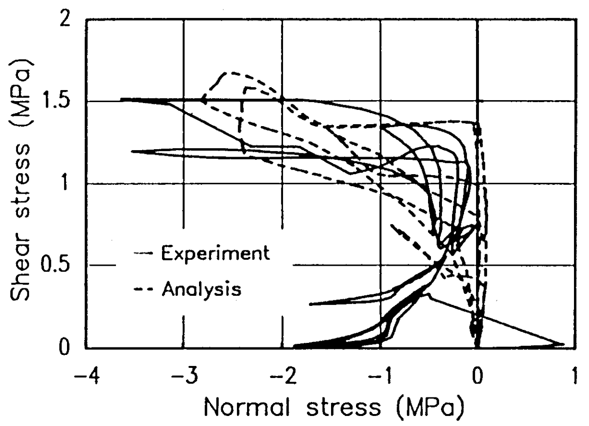

Fig.25 Comparison of Stress Transferred in Concrete

Table 3 Results of Shear Strength Analysis of Orthogonally Reinforced Specimen

No.	Name	$f'c$ (MPa)	Steel yield stress (MPa)	Reif. ratio p (%)	Normal stress σ (MPa)	Steel diameter (mm)	Anal. result τ a (MPa)	Test result τ e (MPa)	τ a/τ e	failure* mode
1		41.6	339.5	1.267	0	19	8.95	7.88	1.14	Y
2		41.6	368.2	1.267	0	13	9.39	9.20	1.02	Y
3		21.5	368.2	1.267	0	13	8.40	6.20	1.35	Y
4		41.1	339.5	2.534	0	19	12.76	10.83	1.18	Y
5		41.1	368.2	2.534	0	13	13.38	11.56	1.16	Y
6		21.5	368.2	2.534	0	13	11.17	8.60	1.30	S
7		43.4	339.5	3.801	0	19	14.74	13.15	1.12	S
8		43.4	368.2	3.801	0	13	15.55	13.65	1.14	S
9	Yamada	24.9	368.2	3.801	0	13	12.72	9.57	1.33	S
10	and	43.5	368.2	5.068	0	13	16.21	14.30	1.13	S
11	Aoyagi	43.5	339.5	5.068	0	19	15.44	13.12	1.18	S
12		39.9	371.4	0.317	0	6	4.56	4.64	0.98	Y
13	($\sigma = 0$)	41.7	371.4	0.950	0	6	8.14	9.06	0.90	Y
14		39.6	371.4	1.584	0	6	10.54	11.25	0.94	Y
15		41.3	368.2	1.126	0	13	8.81	8.02	1.10	Y
16		39.3	368.2	1.689	0	13	10.82	9.40	1.15	Y
17		40.2	368.2	2.534	0	19	13.14	10.46	1.26	S
18		34.8	339.5	2.250	0	13	11.75	10.23	1.15	Y
19		39.5	368.2	1.267	0	19	9.24	7.88	1.17	Y
20		39.5	368.2	2.535	0	19	13.07	10.23	1.28	S
21		40.4	339.5	1.267	0.28	19	8.58	8.16	1.05	Y
22		39.8	339.5	1.267	0.80	19	7.94	7.52	1.06	Y
23	Yamada	40.9	339.5	1.267	1.53	19	7.01	6.62	1.06	Y
24	and	40.9	339.5	1.267	2.14	19	6.04	5.34	1.13	Y
25	Aoyagi	39.6	339.5	1.267	1.09	19	7.57	7.06	1.07	Y
26		37.6	339.5	1.267	1.74	19	6.56	6.10	1.07	Y
27	($\sigma > 0$)	39.2	339.5	1.267	2.37	19	5.57	5.86	0.95	Y
28		39.2	339.5	1.267	2.66	19	5.07	4.38	1.16	Y
29		39.8	339.5	1.267	2.62	19	5.16	4.43	1.17	Y
30		21.4	349.9	0.442	0	9.5	4.74	4.07	1.17	Y
31		21.4	349.9	0.884	0	9.5	6.80	4.68	1.45	Y
32		27.0	349.9	1.326	0	9.5	8.77	5.79	1.51	Y
33		27.0	349.9	1.768	0	9.5	10.17	6.89	1.48	Y
34		28.8	349.9	2.210	0	9.5	11.48	8.97	1.28	Y
35		28.8	349.9	2.670	0	9.5	12.59	9.56	1.32	Y
36		27.8	345.0	0.100	0	3.2	2.49	1.66	1.50	Y
37		27.6	392.0	0.139	0	6.4	4.96	3.59	1.38	Y
38		21.4	349.9	0.884	0	9.5	6.80	4.68	1.45	Y
39	Mattock	27.8	325.4	1.570	0	12.7	9.24	7.09	1.30	Y
40	and	27.8	292.0	2.460	0	15.9	10.95	7.95	1.38	Y
41	Hawkins	28.0	455.7	0.442	0	9.5	5.65	4.85	1.17	Y
42		28.0	455.7	0.884	0	9.5	8.12	6.75	1.20	Y
43	($\sigma = 0$)	29.9	455.7	1.326	0	9.5	10.18	8.13	1.25	Y
44		29.9	455.7	1.768	0	9.5	11.75	9.65	1.22	Y
45		23.4	455.7	2.210	0	9.5	11.76	9.09	1.29	S
46		16.9	349.9	0.442	0	9.5	4.55	3.52	1.29	Y
47		18.0	349.9	0.884	0	9.5	6.62	4.82	1.37	Y
48		16.5	349.9	1.326	0	9.5	8.07	5.59	1.44	Y
49		17.8	349.9	1.768	0	9.5	9.49	5.48	1.73	Y
50		18.0	349.9	2.210	0	9.5	10.57	6.96	1.52	Y
51		26.5	355.3	1.080	0	9.5	7.90	6.05	1.31	Y
52		28.9	343.7	1.570	0	9.5	9.58	6.78	1.41	Y
53		28.9	357.4	1.080	0.69	9.5	7.48	6.37	1.17	Y
54	Mattock	27.1	361.5	1.080	1.12	9.5	6.64	4.90	1.36	Y
55	and	26.2	346.4	1.080	1.37	9.5	6.03	4.62	1.31	Y
56	Hawkins	27.5	358.8	1.080	2.06	9.5	5.18	3.62	1.43	Y
57		27.3	349.2	1.080	2.74	9.5	4.13	2.53	1.63	Y
58	($\sigma > 0$)	26.7	351.9	1.570	1.37	9.5	8.19	5.75	1.42	Y
59		28.5	354.7	1.570	2.74	9.5	6.62	5.52	1.20	Y

* Analytical failure mode : S=Shear failure , Y=Steel yielding

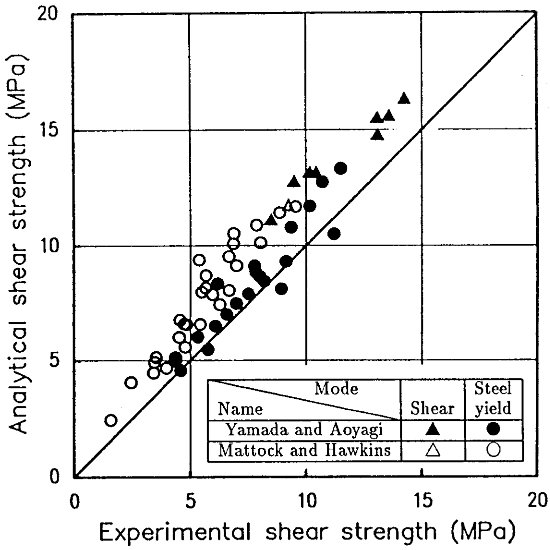

Fig.26 Comparison of Shear Strengths of Orthogonally Reinforced Specimens

is less accurate in the shear slip failure mode for heavily reinforced concrete.

Less accurate prediction brought by the proposed model is attributed to the tensile capacity of reinforcement at the crack. It was reported that the axial mean stiffness and strength of reinforcement deteriorate due to the local curvature at steel sections inside concrete, which is induced by the shear slip along a crack[18]. The fact that the steel cannot fully work up to the pure uniaxial yield strength may be associated with the lower shear strength of reinforced concrete cracks. The reduced axial stiffness of embedded steel originates from the 3-dimensional aspect of reinforcement. Thus, there exists some limit of applicability in terms of the 1-dimensional idealization of reinforcement adopted in this model. Further improvement is now being undertaken by the authors.

5.2 Diagonal reinforcement

Figure 27 compares the results of one of the push-off tests[17] conducted by Yamada and Aoyagi, in which the angle between the reinforcement and a crack surface was taken as the parameter, with the results of analysis. Since the reinforcement ratio of the specimens used in the test is not very high ($p^* = 1.27\%$), the results of the analysis agree relatively well with the test results.

When the angle between the reinforcement and the crack surface is small, as in the case of the specimen with a reinforcement angle of 30 deg., differences from test results tend to be small. However, the influence of reinforcement that meets a crack surface at angles smaller than 30 deg. on the mechanical properties of the crack surface is small. It can be said, therefore, that when the reinforcement ratio is low, as in this test, the model is accurate enough for engineering purposes, even when it is applied to crack surfaces with diagonal reinforcement.

6 CONCLUSIONS

In this study, material models constituting the reinforced concrete discrete crack model have been constructed by modeling slip characteristics of reinforcing steel at a crack surface and stress transfer characteristics of concrete. The reinforcement model has been expanded into a cyclic model for reversed cyclic loading on the basis of the results of the reinforced concrete plate test carried out in this study. Thus, sufficient accuracy of the model when applied to compressive loading after yielding of reinforcement has also been confirmed. A generalized concrete model applicable to any loading history

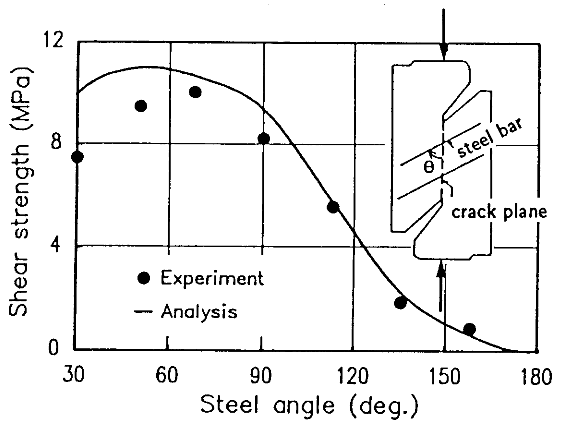

Fig.27 Comparison of Shear Strengths of Diagonally Reinforced Specimens

has also been developed by integrating models of concrete before and after cracking. Furthermore, verification of the discrete crack model as a whole has been conducted. Through the comparison with RC plates and pure shear tests, it has been shown that the model can accurately estimate the deformational behavior and strength of the RC crack plane.

The conclusions of this study are as follows:

(1) A model of the slip of reinforcing steel out of a crack surface and a model of stress transfer in concrete have been formulated as material models constituting the proposed discrete crack model.

(2) The steel strain-slip model proposed by Shima et al. has been expanded into a reversed cyclic model that can express the influence of adjacent cracks, has enhanced accuracy when applied to compressive loading after yielding of reinforcement, and is applicable to the slip of reinforcing steel out of a crack surface in reinforced concrete.

(3) As for loads in the direction perpendicular to the crack surface, such as RC plate tests, shear deformation under reversed cyclic loading and the behavior and strength under unloading and reloading of reinforced concrete members having concrete compressive strengths of 18-40 MPa, with angles of intersection with reinforcing steel of 30-150 degrees, reinforcement ratios of 2% and orthogonal reinforcement in two directions can be estimated with an accuracy of about 10%.

(4) As for pure shear loads in the direction parallel to the crack surface, the the strength under monotonic loading of reinforced concrete members with angles of intersection with reinforcing steel of 30-150 deg., concrete compressive strengths of 17-41 MPa, reinforcement ratios of 2%, and a failure mode in which reinforcing steel fails first can be estimated with an accuracy of 10%. The averages of calculated strength, however, are several percent greater than measured strengths.

(5) Under the same conditions as those in (4) above except at reinforcement ratios exceeding 2% and in a failure mode where reinforcing steel does not fail first, deformation behavior can be estimated accurately if shear stress is about 5 MPa or less. Calculated strengths, however, turned out to be about 20-50% higher than test results.

The differences between calculated values and measured values are due to the analytical model's inability to explain actual phenomena. One of the possible reasons that the average strengths are slightly greater than test results is the degree of anchoring of individual reinforcing bars. In reality, the strength of identical specimens varies depending on the dimensions of specimens, anchorage length of reinforcing steel, presence or absence of anchoring plates, and reinforcement detailing. The results of the analyses conducted here (where infinite anchorage length was assumed) agree well with the results of tests in which the anchorage condition is considered to be good. Criteria for quantifying reinforcement detailing and the degree of anchoring, which are not covered here, remain to be established.

One of the possible causes of lower accuracy in estimating shear strength at higher reinforcement ratios is an insufficient accuracy of the shear transfer model under high shear stresses. However, it has been confirmed, through verification at material level, that deformation characteristics under high restraint and high shear stress can be estimated accurately. Since high shear strengths exceeding 10 MPa can be estimated accurately in a failure mode in which reinforcing steel fails first, it is unlikely that the above cause is a deciding factor.

In the case of highly reinforced concrete in which the crack opening is small for the shear slip, reinforcing steel is thought to be subjected to high local bending and shear deformation. These results indicate that the axial restraining effect of reinforcing steel given by the model (perfect 1-dimensional model) can be reduced by the non-1-dimensional behavior of reinforcing steel. This may be the length to which the method of modeling reinforcing steel as a one-dimensional element can go. This point will be further investigated in a future study.

References

[1] Okamura,H. and Maekawa,K.: Non-linear finite element analysis of reinforced concrete, Proceedings of JSCE, No.360/V-3, pp.1-10, August 1985.(in Japanese)

[2] Shin,H., Maekawa,K. and Okamura,H.: Analytical approach of RC members subjected to reversed cyclic in-plane loadings, Proc. of JCI colloquium on ductility of concrete structures and its evaluation, pp.2(45)-2(56),March 1988. (in Japanese)

[3] Shin,H.: Finite Element Analysis of Reinforced Concrete Members Subjected to Reversed Cyclic In-Plane Loadings, Doctoral dissertation, Department of Civil engineering, The University of Tokyo, 1988. (in Japanese)

[4] Shima,H. Chou,L. and Okamura,H. : Micro and macro models for bond behavior in reinforced concrete, Journal of the Faculty of Engineering, The University of Tokyo(B), Vol.39, No.2, 1987.

[5] Li,B., Maekawa,H. and Okamura,H. : Contact density model for stress transfer across cracks in concrete, Journal of the Faculty of Engineering, The University of Tokyo(B), Vol. XL, No.1, 1989.

[6] Mishima,T. Yamada,K. and Maekawa,K. : Localized deformational behavior of a crack in RC plates subjected to reversed cyclic loads, Proceedings of the Japan Society of Civil Engineers, No.442/V-16,pp.161-170, February 1992.(in Japanese)

[7] Bujadham,B. and Maekawa,K. : The universal model for stress transfer across cracks in concrete, Proceedings of the Japan Society of Civil Engineers, No.451/V-17,pp.277-287, August 1992.

[8] Goto,Y. : Cracks formed in concrete around deformed tension bars, Journal of ACI, Vol.68, pp.244-251, April 1971.

[9] Kato,B. : Mechanical properties of steel under load cycles idealizing seismic action, Bulletin D'Information No.131, CEB, AICAP-CEB symposium, Rome, pp.7-27, 1979.

[10] Lim,T.B. Li,B. and Maekawa,K. : Mixed mode strain-softening model for shear fracture band of concrete subjected to in-plane shear and normal compression, Proceedings of the International Conference on Computational Plasticity, Barcelona, pp.1431-1444, April 1987.

[11] Maekawa,K. Niwa,J. and Okamura,H. : Computer program COMM2 for analyzing reinforced concrete, Proceedings of the JCI 2nd colloquium on analytical studies on shear design of reinforced concrete structures, JCI, pp.79-86,October 1983. (in Japanese)

[12] Aoyagi,Y. and Yamada,K. : Strength and deformation characteristics of RC shell elements subjected to in-plane forces, Proceedings of the Japan Society of Civil Engineers, No.331,pp.167-180, March 1983. (in Japanese)

[13] Chou,L. Yamao,S. and Okamura,H. : Strain distribution of steel bars in footing, Proc. of JCI, Vol.4, pp.417-420, 1982. (in Japanese)

[14] Niwa,J., Chou,L. Shima,H. and Okamura,H. : Nonlinear spring element for strain-slip relationship of a deformed bar, US-JAPAN Seminar on Finite Element Analysis of Reinforced Concrete Structures, Vol.2, pp.227-235, 1985. (in Japanese)

[15] Ideguti H., Matsumoto S. and Maemura M. : Study on distribution of plastic strain along a steel bar subjected to reversed cyclic loading and calculating of the steel slip, Proceedings of the 43rd annual conference of JSCE, 5, pp.630 -631, 1988.(in Japanese)

[16] Mattock,A.H. and Hawkins,N.M. : Shear transfer in reinforced concrete-resent research, Journal of PCI, Vol.17, No.2, pp.55-75, March-April 1972.

[17] Yamada,K. and Aoyagi,Y. : Shear transfer along cracks, Proceedings of the JCI 2nd colloquium on analytical studies on shear design of reinforced concrete structures, JCI, pp.19-26,October 1983.(in Japanese)

[18] Maekawa,K., Khan,J., Qureshi,J. and Mishima,T. : Reduced axial stiffness of deformed bars under shear slip along a crack in concrete, Bond in Concrete, CEB, Latvia, Oct. 1992.